ORIGINAL PAPER

Micro-scale flood risk analysis based on detailed 2D hydraulic modelling and high resolution geographic data

**Julien Ernst · Benjamin J. Dewals · Sylvain Detrembleur ·
Pierre Archambeau · Sébastien Erpicum · Michel Pirotton**

Abstract The paper presents a consistent micro-scale flood risk analysis procedure, relying on detailed 2D inundation modelling as well as on high resolution topographic and land use database. The flow model is based on the shallow-water equations, solved by means of a finite volume scheme on multi-block structured grids. Using highly accurate laser altimetry, the simulations are performed with a typical grid spacing of 2 m, which is fine enough to represent the flow at the scale of individual buildings. Consequently, the outcomes of hydraulic modelling constitute suitable inputs for the subsequent exposure analysis, performed at a micro-scale using detailed land use maps and geographic database. Eventually, the procedure incorporates social flood impact analysis and evaluation of direct economic damage to residential buildings. Besides detailing the characteristics and performance of the hydraulic model, the paper describes the flow of data within the overall flood risk analysis procedure and demonstrates its applicability by means of a case study, for which two different flood protection measures were evaluated.

Keywords Flood risk analysis · Micro-scale · Inundation modelling ·
Land use maps · Digital surface model · Finite volume

J. Ernst, B. J. Dewals have contributed equally to this article.

J. Ernst · B. J. Dewals (✉) · S. Detrembleur · P. Archambeau · S. Erpicum · M. Pirotton
Department ArGEnCo, Unit of Hydrology, Applied Hydrodynamics and Hydraulic Constructions,
University of Liege, Liege, Belgium
e-mail: B.Dewals@ulg.ac.be

J. Ernst
e-mail: J.Ernst@ulg.ac.be

M. Pirotton
e-mail: hach@ulg.ac.be
URL: www.hach.ulg.ac.be

1 Introduction

Global circulation models (GCM) and regional climate models (RCM) provide estimates of the possible changes in precipitation and evapotranspiration patterns as a result of climate change. Hydrological modelling may be used subsequently for translating those changes in climate parameters into changes in river discharges, accounting for expected evolutions in land use. Those projections remain affected by a significant level of uncertainty due to the climate and hydrological models themselves and, to a greater extent, to the discrepancies in the scenarios used for running those models (IPCC 2007).

Nevertheless, in a number of river basins, models predictions converge towards a clear increase in peak discharges both in terms of intensity and frequency. Therefore, managing flood risk will remain an issue of primary importance and will increasingly require suitable flood protection strategies. Moreover, flood risk management is currently shifting from the full protection against flooding towards the management of the consequences of flooding (Coninx and Bachus 2007). The selection of cost-effective combinations of flood reduction measures and the identification of means to reduce flood consequences should rely on a risk-based approach, taking into consideration not only purely technical criteria but also economic, social and environmental factors. In addition, the analysis should be conducted at a sufficiently detailed resolution.

The present paper depicts a modelling chain, combining detailed two-dimensional inundation modelling with high resolution and highly accurate land use data to evaluate the exposure and the inundation risk, both in terms of social impact and economic damage. Environmental aspects are not yet incorporated in the analysis, presently focused on urbanized areas.

While such risk analyses are mostly undertaken at a macro- or meso-scale (FloodSite 2005), the herein described analysis is performed at a micro-scale, meaning that the considered assets are the individual buildings or facilities. Such a refined analysis is relevant to reliably assess the effectiveness of local measures for protecting individual inundated areas. It also requires an overall consistency in terms of resolution and accuracy between the expected results and both the flow modelling approach and available input data (Apel et al. 2009). Therefore, taking benefit of recent advances in the availability of data (Van der Sande et al. 2003), accurate land use database is exploited to identify each building or facility individually and to characterize their vulnerability, using a social vulnerability index and economic damage function. In addition, a two-dimensional flow model is used to provide high resolution flood maps detailing the distribution of water depth and flow velocity in the floodplains as well as representing the hydrodynamic interactions between the main channel and the floodplains.

The hydraulic model is based on the fully dynamic shallow-water equations solved by means of a finite volume technique. Multi-block Cartesian grids are exploited, enabling local mesh adaptation, while an automatic mesh refinement tool embedded in the hydraulic model leads to significant reductions in computation time for simulating steady flows. Consistently with the high resolution digital surface models (airborne laser altimetry) exploited to represent the floodplains, computational grids as fine as 2 m by 2 m are used to conduct the hydraulic simulations, leading to accurate predictions of the flow pattern at the scale of individual buildings. The obtained hydraulic results serve as direct input for the subsequent exposure and risk analyses.

An overview of the risk modelling chain is provided in the next section, while the 2D hydraulic model is presented in Sect. 3. Next, Sect. 4 details the exposure evaluation and shows how the inundation characteristics are combined with vulnerability data to estimate

the risk. Finally, Sect. 5 discusses the application of the modelling chain for a specific case study involving the assessment of flood reduction measures along river Ourthe in the Meuse basin (Belgium).

2 Overview of the risk analysis procedure

Flood risk is usually defined as the expectation value of losses due to flood hazard. Following Kaplan and Garrick (1981), a more general expression of risk is the *risk curve* itself (and not only its mean), showing the complete relationship between flood frequency and flood damage.

The risk curve is given by the set of N pairs (T_i^{-1}, D_i), with D_i the amount of damage or impact (Euros, affected people…), T_i^{-1} the corresponding flood frequency (or exceedance probability) and N the number of flood events considered. The expectation value of damage $\langle D \rangle$ is obtained by integrating the risk curve. Using the composite trapezoidal rule for this purpose leads to the following expression:

$$\langle D \rangle = \sum_{i=1}^{N} \left[\left(\frac{1}{T_{i-1}} - \frac{1}{T_i} \right) \frac{D_{i-1} + D_i}{2} \right]. \tag{1}$$

Following both definitions, risk has three components, namely hazard, exposure and vulnerability. Flood hazard is given by the intensity of inundation for flood events of different return periods (or frequencies), as expressed by the spatial distribution of water depth and flow velocity obtained here from the 2D flow model. Exposure evaluation refers to the identification of all buildings, structures and people affected by the hazard. Vulnerability is the degree of damage the assets would encounter if flood occurs. Commonly, flood damage is related to the depth, velocity, duration and extent of flooding. In the present analysis, the three main components of flood risk are sequentially evaluated following the procedure detailed in Fig. 1, which also highlights input data such as hydrological statistics, topography, land use, value and susceptibility of the assets. The procedure involves basically the four steps described below:

1. flood hazard identification: using a number of different river discharge values, of known return periods, 2D hydraulic modelling is performed to provide detailed inundation characteristics;
2. exposure evaluation: based on a geomatic analysis, flow characteristics are combined with high resolution land use data to evaluate the exposure, i.e. (1) identify the affected assets for each return period, both in terms of affected people and affected buildings or facilities and (2) assign inundation characteristics (mainly water depth) to each affected asset;
3. assessment of social vulnerability and risk: third, considering the social vulnerability of affected people, the inundation characteristics enable to deduce the social impacts for each return period and thus the social risk;
4. assessment of economic vulnerability and risk: similarly, using an appropriate flood loss model as well as estimates of the value of the affected buildings and facilities, the direct economic damage is estimated for each return period, together with the corresponding economic risk.

The social vulnerability of people is appreciated by means of a composed index developed by Coninx and Bachus (2007) and based on socio-economic data at the level of
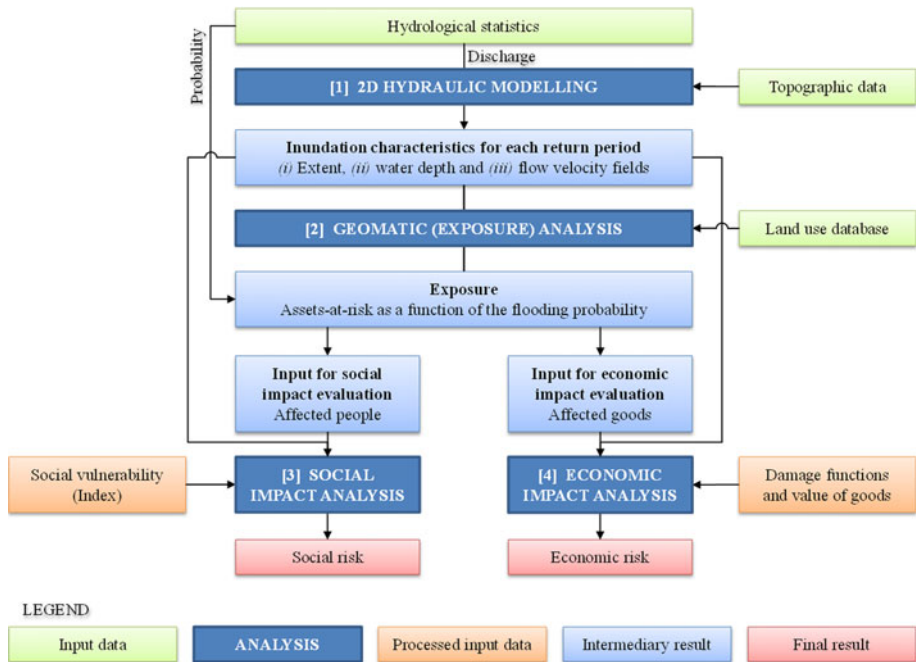
Fig. 1 Methodology and flow of data for hydraulic modelling, exposure analysis and risk evaluation

statistical districts. Next, this vulnerability index is combined with the adaptive capacity of the community and the inundation characteristics to obtain the social risk (Coninx 2008; Ernst et al. 2009b), expressed by the relationship between flood frequency and corresponding level of social impact as well as by maps showing its spatial distribution.

As regards economic risk evaluation, the analysis presently focuses on direct damage to housing, reported as the main component of total flood damage in the case study of interest. Estimates of the value of the assets are deduced from a sample of property values in the case study area. They are combined with an existing flood loss model to appreciate economic damage and risk.

3 Hazard analysis

The aim of hazard analysis is to evaluate the intensity of a number of inundation scenarios and to associate a flood frequency to each of them. It consists thus in transforming the discharge associated with defined return periods into inundation extent, water depths and flow velocities by means of a hydraulic model.

3.1 Model description

The complex interactions between the main channel and the floodplains during floods are important flow features and may not be neglected (McMillan and Brasington 2008). 1D flow models or excessively simplified 2D models are unable to reproduce satisfactorily the mass and momentum exchanges between these two flow areas, especially when densely

urbanized floodplains are concerned. Therefore, simulations of floodplain inundation flows are conducted here with the two-dimensional numerical model *WOLF 2D*, developed at the University of Liege (Dewals et al. 2006a, b, 2008c; Erpicum et al. 2009a, b; Erpicum et al. 2010).

Similar detailed models have been used by other authors, such as Mignot et al. (2006) or Begnudelli et al. (2008), whereas many studies have been conducted based on simplified 2D solvers (e.g. Bradbrook et al. 2005) or approaches coupling models of different levels of complexity in the channel and the floodplain (Bates and de Roo 2000; McMillan and Brasington 2007).

3.1.1 Mathematical model

The model is based on the conservative form of the depth-averaged equations of mass and momentum conservation, namely the "shallow-water" equations (Chaudhry 1993). Bottom friction is conventionally modelled using an empirical law, such as Manning formula. The model enables the definition of a spatially distributed roughness coefficient and provides the additional possibility to reproduce friction along side walls by means of a process-oriented formulation (Dewals et al. 2008c; Erpicum et al. 2009b; Roger et al. 2009). The increase in friction area as a result of irregular topography is accounted for consistently with Hervouet (2003) and Wu (2008).

3.1.2 Computational implementation

Multi-block Cartesian grids are used. They enable local mesh refinement close to areas of particular interest, while preserving the lower computational cost required by Cartesian compared to unstructured grids for the same order of accuracy.

The space discretization is performed by means of a finite volume scheme, achieving second-order space accuracy. A flux vector splitting (FVS) technique developed by the authors has been used. Besides requiring low computational cost, this FVS offers the advantages of being Froude-independent and of facilitating a satisfactory adequacy with the discretization of the bottom slope term (Erpicum et al. 2009a, 2010). This FVS has already proven its validity and efficiency for numerous applications (Dewals et al. 2006a, b, 2008c; Erpicum et al. 2007, 2009b; Roger et al. 2009).

Since the model is applied to compute steady-state solutions, as detailed in Subsect. 3.2, the time integration is performed by means of a three-step first-order accurate Runge–Kutta algorithm. The time step is constrained by the Courant-Friedrichs-Levy condition. A semi-implicit treatment of the bottom friction term is used, without requiring additional computational cost (Caleffi et al. 2003).

3.1.3 Mesh adaptation and automatic grid refinement

A grid adaptation technique is used to restrict the computation domain to the wet cells. Wetting and drying of cells are handled free of mass conservation error by means of an iterative resolution of the continuity equation.

In addition, the model includes an *automatic mesh refinement* algorithm (AMR). For steady-state simulations, the AMR tool consists in performing the computation on several successive grids, starting from a coarse one and gradually refining it up to the finest one. When the flow field is stabilized on one grid, the solver automatically jumps onto a finer

one. The successive solutions are interpolated from the coarser towards the finer grid. This fully automatic method considerably reduces the number of cells in the first grids, while increasing the time step, and thus substantially reduces the total run time, despite slight extra computation time required for meshing and interpolation operations (Dewals et al. 2008a; Erpicum et al. 2010).

3.2 Model application

3.2.1 Topographic data

High resolution and highly accurate topographic datasets have become increasingly available for inundation modelling in a number of countries. In Belgium, a data collection programme using airborne laser altimetry (LIDAR) has generated high quality topographic data covering the floodplains of most rivers in the southern part of the country. Simultaneously, the bathymetry of these rivers has been surveyed by means of an echo-sonar technique. Consequently, combining data generated from those two remote sensing techniques enables to obtain a complete digital surface model (DSM) characterized by a horizontal resolution of 1 m by 1 m and a vertical accuracy of 15 cm.

Those high quality topographic data combined with simulations performed on grids as fine as 2 m by 2 m enable to conduct inundation modelling at the scale of individual streets and houses. The fine mesh also enables to set the value of roughness coefficients to represent only small scale roughness elements and not to globalize larger scale effects such as blockage by buildings. As a result, wide ranges of discharges may be simulated without the need for recalibration of the roughness parameter.

3.2.2 Steady-state assumption

The case study considered hereafter is situated in the central part of the Meuse basin, the morphological and hydrological characteristics of which enable to assume a steady flow at the scale of a river reach. Indeed, as detailed by de Wit et al. (2007), the Meuse basin can be subdivided into three major geological zones, referred to as "Lotharingian Meuse" (southern part), "Ardennes Meuse" (central part) and the Dutch and Flemish lowlands (northern part). The southern and northern parts are characterized by wide floodplains where flood waves are significantly attenuated. In contrast, in the central part of the Meuse basin, the rivers are captured in the Ardennes massif, characterized by narrow steep valleys.

As shown by de Wit et al. (2007), the tributaries of river Meuse in the Ardennes Massif present large river bed gradients, combined with relatively narrow cross-sectional shape of the valleys, leading to very low storage capacity in the floodplains. As a result, the floodplains get completely filled with water quickly after the beginning of the flood, and a quasi-steady inundation flow is then observed.

For instance, for typical floods occurring on river Ourthe (Sect. 5), it has been verified that the volume of water stored in the floodplains along a 10-km-long reach remains lower than 1% of the total amount of water flowing in.

In addition, comparisons have been made between inundation patterns predicted by unsteady flow simulations, for which the real flood hydrograph is prescribed as an upstream boundary condition, and inundation patterns computed assuming a steady-state flow (constant discharge close to the peak discharge of the hydrograph). Those comparisons have

confirmed that the maximum flood extents predicted by both approaches are in very good agreement.

Therefore, a steady-state assumption has been considered as valid for simulating floodplain inundation along most rivers of the Ardennes Massif. It has thus been systematically used in the simulations discussed in the subsequent paragraphs. An additional benefit of this assumption is a reduced run time and the possibility to exploit automatic mesh refinement (Subsect. 3.1).

3.2.3 Validation

Since 2003, the flow model *WOLF 2D* has been applied to conduct inundation modelling along more than 1000 km of rivers in the southern part of Belgium, based on detailed topographic data. Within this framework, the inundation model has been validated by comparison of the numerical results with observed flood extents and measured water depths during recent flood events. Reference data were obtained at gauging stations, collected by field surveys or deduced from aerial pictures of the flood, as shown in the validation examples detailed by Erpicum et al. (2010). Predictions of water surface elevation were found to have a mean absolute error in the range 10–15 cm.

4 Exposure, vulnerability and risk analyses

4.1 Available data

In order to deduce the exposure and the flood impacts from the inundation characteristics, high resolution land use database and other geo-referenced datasets have been exploited, consistently with the micro-scale approach followed throughout the present analysis. The geometric and semantic characteristics of these datasets are briefly described hereafter and summarized in Table 1.

There are basically two accurate land use vector database available for the southern part of Belgium: *Top10v-GIS* and *PICC*, respectively, provided by the Belgian *National Geographic Institute* (IGN) and the *Service Public de Wallonie* (SPW). The former contains 18 different layers of information, such as land use, structures or hydrographical network, while the later is based on stereoscopic aerial imagery restitution and a manual post-processing consisting in enhancements such as house numbering and street names. They constitute two complementary high resolution datasets (scale: 1:10,000), which have been combined in the exposure analysis to achieve an optimal identification of the assets (geometric feature) and of their type (semantic feature). Since PICC enables to identify

Table 1 Main characteristics of the geo-referenced datasets exploited as input for the risk analysis procedure

Data set	Format	Geometric quality	Semantic quality	Use in the risk analysis procedure
LIDAR	Raster	High	Low	Hydraulic modelling: topography
Top10v-GIS	Vector	High	High	Exposure analysis: type of assets
PICC	Vector	High	High	Exposure analysis: identification of assets
Statistical data	Vector	Low	High	Input for the social vulnerability index
Land registry	Vector	Medium	High	Input for estimating the value of the assets

each house individually, while Top10v-GIS does not, the former has been exploited for the identification of the assets, whereas the later, containing richer information on land use categories, has been used to determine the type of affected assets.

The Belgian *National Institute of Statistics* (INS) provides database including socio-economic information needed for the evaluation of the social exposure and vulnerability (Subsect. 4.3), such as the number of inhabitants per statistical district as well as the number of elderly or financially deprived people, single parents or non-European residents. A statistical district covers typically 0.25–1 km^2 and is the smallest level at which such socio-economic data are available. The latest Belgian national socio-economic population survey dates back to 2001.

The *Land registry* geographic database lists all private properties with their cadastral income, which constitute necessary inputs to estimate the economic value of the assets. Although geo-referenced, the land registry is characterized by a significantly lower geometric accuracy compared to *Top10v-GIS* and *PICC*. Therefore, land registry data are only exploited for their semantic contain.

Among these datasets, none of them contains information about people location in the area at risk. But the combination of these datasets and the assumption that the number of people living in each residential building in a given statistical sector remains the same leads to an estimation of the location of people at risk.

4.2 Exposure evaluation

The next step after hydraulic modelling consists in identifying the people and assets affected by the inundation, based on a combination of inundation extent and geographic database PICC. Next, based on database Top10vGIS, each affected asset is classified into a category such as residential, public, commercial or industrial building, road or railway network…

Practically, based on the PICC information, each affected residential building is located and assigned a unique identifier. In parallel, an attribute value table is created to store all information about these buildings, such as street name, postal number and results.

Since the flow simulations are conducted based on a DSM, including over grounded structures, such as buildings, and not a Digital Terrestrial Model, water depths computed at the location of an inundated building remains always zero, except if the building would be overtopped, which would only occur for extreme flow conditions such as induced by dam break. A building is thus assumed to be affected by the inundation if neighbouring cells are wet (Fig. 2).
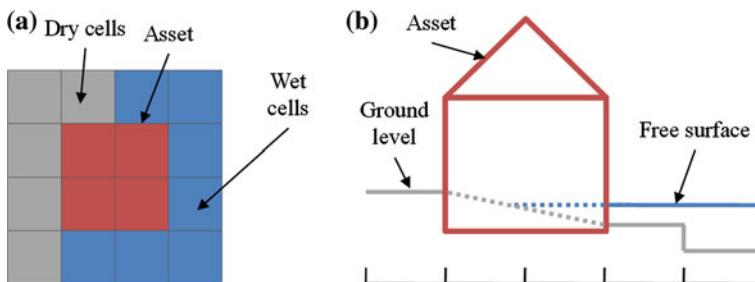
Fig. 2 Sketch of the estimation of water depth inside buildings affected by the inundation: (**a**) plane view and (**b**) vertical view

Consequently, water depth and other flow characteristics affecting the buildings are not a direct result from hydraulic modelling, but they need to be computed by a specific post-processing. This assignment of flow characteristics (water depth and flow velocity) to each building may be performed in two different ways. Either the water depth in the building is obtained by averaging the water depth in the neighbouring cells; or the ground level and the free surface elevation are linearly interpolated inside the asset, based on a least square approximation, to deduce a mean water depth inside the building, as sketched in Fig. 2b. Both methods lead to similar results and may also be applied for estimating the flow velocity affecting each building.

To evaluate the number of people living in each house, the procedure relies on the following sub-steps: first, the number of residential buildings in each statistical sector is evaluated; next, since the number of people living in the sector is known, the average number of people living in each residential building can be estimated and recorded in the attribute value table.

Once the affected buildings are identified and based on the inundation characteristics, the following *flood-exposure index FI* [-], needed for the social impact assessment, may be evaluated (Coninx 2008; Ernst et al. 2009a, b):

$$FI = 0.45\ WD + 0.22\ WR + 0.22\ V + 0.11\ D \tag{2}$$

where WD = water depth score [-], WR = water rise score [-], V = velocity score [-] and D = duration score [-]. Each of these scores is binary valued (0 or 1) depending on a threshold. As regards the water depth, the threshold value is 0.3 m. For the velocity, the threshold value is 2 m/s, 12 h for flood duration (Penning-Rowsell et al. 2003), whereas the water rising rate has to be appreciated as slow or sudden in comparison with warning and evacuation time.

4.3 Vulnerability and risk analysis

Since the purpose of the present paper is to focus primarily on how the detailed hydraulic simulations are combined with high quality geographic database to conduct exposure analysis, the social and economic impact analyses are only briefly described. For further details, the reader is referred to the cited references.

4.3.1 Social vulnerability and appreciation of social impact

Three main aspects need to be considered when evaluating social impacts of a given flood scenario, namely (1) the inundation characteristics provided by hydraulic modelling, (2) the vulnerability of the people themselves and (3) the adaptive capacity of the community (Coninx and Bachus 2007; Coninx 2008; Ernst et al. 2009b).

The *vulnerability* of people depends on their socio-economic characteristics as well as on their ability to decrease their susceptibility and to recover from flooding. As developed by Coninx and Bachus (2007), social vulnerability is appreciated here by means of a composed index V [-], which depends on six indicators X_i [-] equal to the ratios of (1) elderly, (2) ill people, (3) lone parents, (4) foreigners, (5) financially deprived people, and (vi) people living in one-storey houses. The indicators are aggregated by the geometric mean and equally weighted (Ernst et al. 2009b):

$$V = 1 - \prod_{i=1}^{6} (1 - X_i) \tag{3}$$

This index is used to identify four categories of social vulnerability: (1) resilient ($0 < V < 0.06$), (2) weakly vulnerable ($0.06 < V < 0.13$), (3) vulnerable ($0.13 < V < 0.19$) and (4) extremely vulnerable ($0.19 < V$).

The *adaptive capacity* of society is also considered since the social flood impacts may be mitigated by preparatory and protective measures. In contrast to vulnerability research, the search for indicators to make adaptive capacity operational is rather new and only few systematic methods seem to approach adaptive capacity. Similarly to Brouwer et al. (2007), Coninx (2008) has developed an analytical framework to quantify the adaptive capacity at the level of Belgian municipalities, reflecting the availability of measures such as private protections, flood forecasting and flood warning or psycho-social support. The analysis is based on several indicators, including existence of technological and non-technological measures, availability and distribution of resources, institutional structure, risk spreading instruments, information and public perception. By scoring these indicators, a total adaptive capacity score AC [-] is obtained (Coninx 2008; Ernst et al. 2009b).

Finally, the flood-exposure index FI is combined with the vulnerability index V and the adaptive capacity score AC, to obtain a *social flood impact index SI* [-] distinguishing between people affected by "low", "medium" and "high" social impacts (Coninx 2008; Ernst et al. 2009b):

$$SI = 0.5\, FI + 0.25\, V + 0.25\, AC. \tag{4}$$

Indeed, due to their intangibility, social flood impacts are hard to quantify separately and it is thus appropriate to use an aggregated index indicating the level of severity of the social flood impacts and enabling relative comparison between areas to prioritize risk reduction needs.

4.3.2 Economic vulnerability and damage evaluation

As an outcome of the exposure analysis, all affected goods have been identified and assigned a type as well as flow characteristics. Next, a relative damage function is applied for each asset to deduce damage as a percentage of its total value. This value is estimated from various sources, such as local authorities or Land Registry data. The present methodology concentrates on direct economic damage to residential buildings.

Damage functions are considered as the standard approach to evaluate flood damage (Smith 1994). They establish a link between induced damages and hydraulic parameters, i.e. mainly water depth and flow velocities (ICPR 2001; Dushmanta et al. 2003; Penning-Rowsell et al. 2003). Other parameters may also be included, such as precautionary measures (Apel et al. 2007), water contamination (Thieken et al. 2008) or flood duration, by distinguishing, for instance, between short (less than 12 h) and long (more than 12 h) duration floods (Thieken et al. 2008).

Although absolute damage functions may also be used (FloodSite 2005), relative damage functions are preferred here because they are easier to transpose from one region to another, provided local estimates of the value of the assets are available (Merz et al. 2004).

Much care is required when selecting and applying a damage function, due to the scattering remaining between the results of the large number of existing functions. Since the present study does not aim at developing new damage functions nor at discussing in

detail the validity of specific functions, the recent *FLEMO* functions were simply used here. They apply for meso- and micro-scale analysis (Thieken et al. 2008). They were fit from a dataset gathered by computer-aided phone consultations to households and companies after the major flood events in August 2002 in Germany (Thieken et al. 2005; Kreibich et al. 2007). For these floods, meso-scale validations have shown that FLEMO outperforms other loss models used in Germany. However, when applied to other flood events FLEMO tends to overestimate the losses (Thieken et al. 2008).

Although a standard methodology is applied here for economic damage evaluation, the analysis remains innovative as a result of the scale at which it is conducted, preserving the detailed distribution of the inundation characteristics provided by the 2D flow model on grids as fine as 2 m by 2 m.

5 Case study

5.1 Description of the case study area

The risk analysis procedure has been applied to a case study, which covers two neighbouring reaches of the lower part of river Ourthe in the Meuse basin (Belgium). These meandering reaches, between the municipalities of Esneux and Tilff, are situated a few kilometres upstream of the mouth of river Ourthe into river Meuse and the corresponding catchment area covers about 2900 km^2 (Fig. 3). The total length of the simulated reaches is 16 km.

Over the past 20 years, four major floods were recorded along the considered part of river Ourthe: (1) in 1993, with a peak discharge of 742 m^3/s; (2) in 1995, 520 m^3/s; (3) in 2002, 570 m^3/s and (4) in 2003, 508 m^3/s. Validation data are thus available but mainly as far as hydraulic modelling is concerned (aerial imagery corresponding to the peak discharge of the flood, measures at gauging stations, field surveys). With the aim of validating the hydraulic modelling for the studied area, these historic flood events were simulated using the flow model presented in Sect. 3 and comparisons similar to those presented by
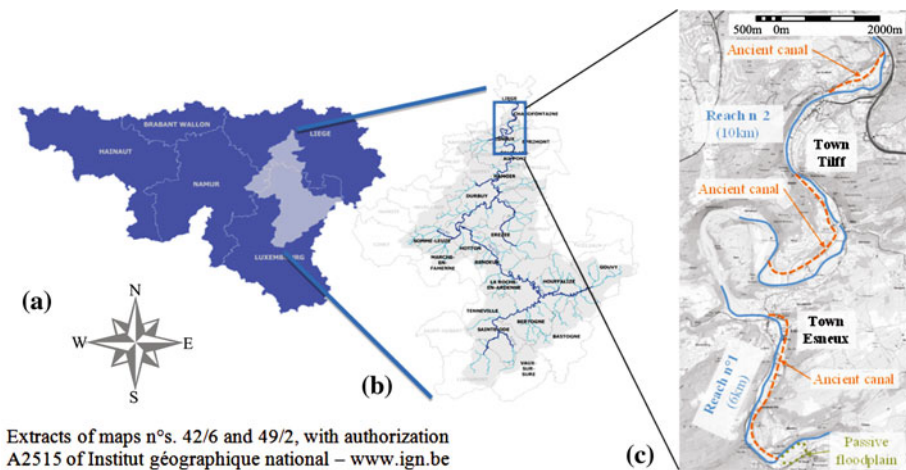
Fig. 3 Location of the case study of river Ourthe: (**a**) Southern part of Belgium, (**b**) Sub-basin of river Ourthe and (**c**) case study area

Erpicum et al. (2010) have shown a very satisfactory agreement between observations and numerical predictions, both in terms of inundation extent and water depths.

Similarly, a survey covering 383 households has provided validation data for the exposure analysis presented in Subsect. 4.2 hereafter (Boquet 2009).

In contrast, reliable data are lacking for validating the socio-economic impact evaluation. In Belgium, the *Disaster Fund* centralizes data about damage induced by natural disasters such as flooding. Compensations claimed by affected people and actually allocated by the state are registered, as well as the number of allegedly flooded houses. However, this recorded number is found significantly lower than the number of houses actually located within the inundation extent deduced from aerial imagery. This discrepancy may result from unregistered private flood protections or from households not undertaking the administrative procedure to claim compensation. As a result, direct validation of economic damage is hardly possible since available data underestimate both exposure and damage. Nevertheless, data from the Disaster Fund have revealed that damage to residential buildings is by far the most important recorded type of damage (Giron et al. 2009).

5.2 Flood risk in the present situation (base scenario)

The risk analysis procedure depicted in Sect. 2 was applied for the case study by performing sequentially hydraulic modelling, exposure analysis and socio-economic impact evaluation.

5.2.1 Hydraulic modelling

For each flood frequency, or return period, the corresponding discharge was used in the detailed 2D hydraulic model as an upstream boundary condition, while measured stage-discharge relationships were used to prescribe the downstream boundary condition.

Hydrological data used for the case study were obtained from a standard statistical analysis of a 30-year-long time series of discharges measured at a nearby gauging station along river Ourthe. As shown in Fig. 4, a two-parameter Gamma distribution was fitted based on the maximum likelihood method ($\alpha = 0.01464$ $(m^3/s)^{-1}$ and $\lambda = 5.809$):

$$f(Q) = \frac{\alpha^\lambda}{\Gamma(\lambda)} Q^{\lambda-1} e^{-\alpha Q} \quad \text{with } \Gamma(\lambda) = \int_0^\infty u^{\lambda-1} e^{-u} du \tag{5}$$

Units of parameter α and probability density f are both $(m^3/s)^{-1}$, while λ is non-dimensional. Figure 4 represents the cumulative Gamma distribution $F(Q) = 1 - T^{-1}$ as well as the associated 95% confidence interval (Table 2). The ten discharge values considered for hydraulic modelling are also marked on the curve (•). Cumulative probability F and flood frequency T^{-1} are both non-dimensional.

As a result of the application of the hydraulic model, based on a grid size of 2 m by 2 m, inundation extent as well as 2D distribution of water depth and depth-averaged velocity components was obtained for each considered discharge (e.g. Fig. 5).

5.2.2 Exposure

Next, the exposure evaluation (Subsect. 4.2) was applied to the results of hazard analysis, as detailed below for the downstream reach of the case study (reach no 2 in Fig. 3). Similar results were found for the upstream part of the case study (reach no 1).
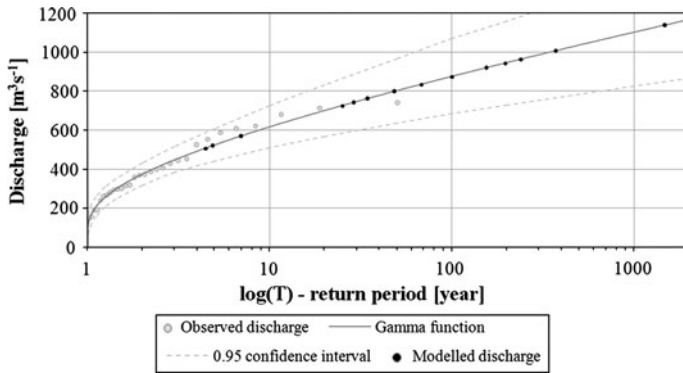
Fig. 4 Cumulative distribution of the discharge as a function of the return period for the case study of river Ourthe, as well as observed discharge values (○) and values considered for hydraulic modelling (●)

Table 2 Considered return periods and corresponding discharges as well as 95%-confidence interval (CI) for the case study of river Ourthe
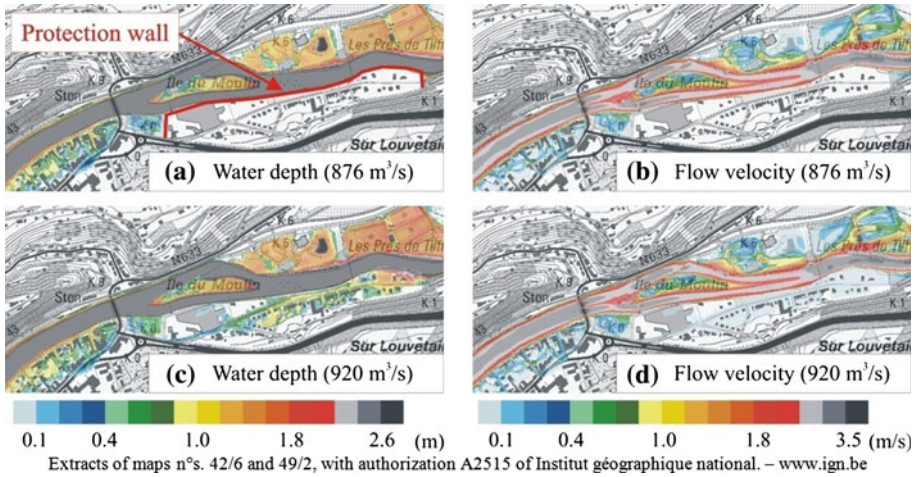
ID	1993	1995	2002	2003	
Return period (years)	29	5	7	4	
Flood frequency (−)	3.5×10^{-2}	2.1×10^{-1}	1.4×10^{-1}	2.2×10^{-1}	
Discharge (m³/s)	742	520	570	508	
ID	Q25	Q25 + 5%	Q25 + 10%	Q25 + 15%	Q25 + 30%
Return period (years)	25	34	48	68	196
Flood frequency (−)	4.0×10^{-2}	2.9×10^{-2}	2.1×10^{-2}	1.5×10^{-2}	5.1×10^{-3}
Discharge (m³/s)	726	762	799	835	944
ID	Q100	Q100 + 5%	Q100 + 10%	Q100 + 15%	Q100 + 30%
Return period (years)	100	154	239	371	1481
Flood frequency (−)	1.0×10^{-2}	6.5×10^{-3}	4.2×10^{-3}	2.7×10^{-3}	6.8×10^{-4}
Discharge (m³/s)	876	920	964	1007	1139

Thanks to the semantic quality of available land use data (Subsect. 4.1), each asset affected by the inundation has been identified individually, including residential and non-residential buildings, as exemplified in Fig. 6 for a 154-year flood. This figure shows that the present micro-scale analysis provides the detailed spatial distribution of affected assets.

Figure 7 shows the number of affected people and corresponding number of affected residential buildings as a function of flood frequency. The latter is not directly proportional to the former since the number of inhabitants per house is not assumed to be constant but is spatially distributed, consistently with the micro-scale approach followed throughout the present analysis. Results of Fig. 7 may alternatively be expressed as a function of the return period (Table 2). The graphs reveal a steeper increase in the exposure for discharge values in the range between 876 m³/s and 920 m³/s, resulting from the overtopping of a flood protection wall designed for the 100-year flood (876 m³/s). The overtopping leads to a sudden increase in the inundation extent and hence in the exposure, as shown in Fig. 5.

The flow characteristics affecting each building were evaluated for each considered discharge, as detailed in Subsect. 4.2. Consequently, the preliminary binary outputs of the

Extracts of maps n°s. 42/6 and 49/2, with authorization A2515 of Institut géographique national. – www.ign.be

Fig. 5 Water depth and flow velocity magnitude simulated for discharges just below (876 m³/s) and just above (920 m³/s) the threshold discharge for overtopping of the existing protection wall
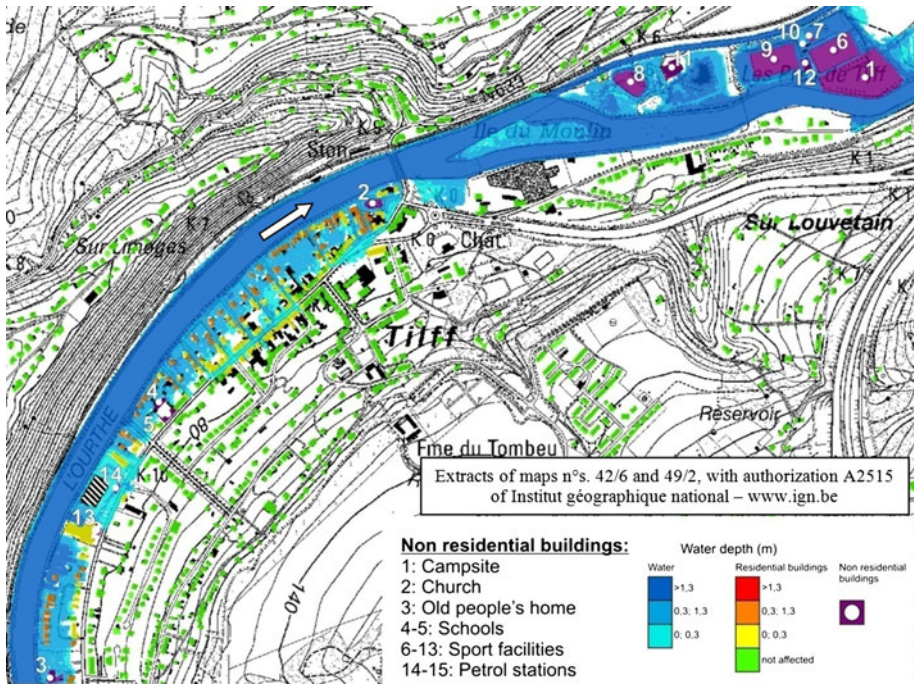
Fig. 6 Spatial distribution of inundation depth (m, *blue colour scale*) and exposure of residential and non-residential buildings (*yellow* to *red colour scale*), for a 154-year flood in the present situation

exposure analysis (i.e. the asset is affected or not) could be enhanced, as illustrated in Fig. 7, where three categories of water depth are emphasized. For discharge values lower than the 100-year flood, hardly any houses undergo flooding with a water depth higher than
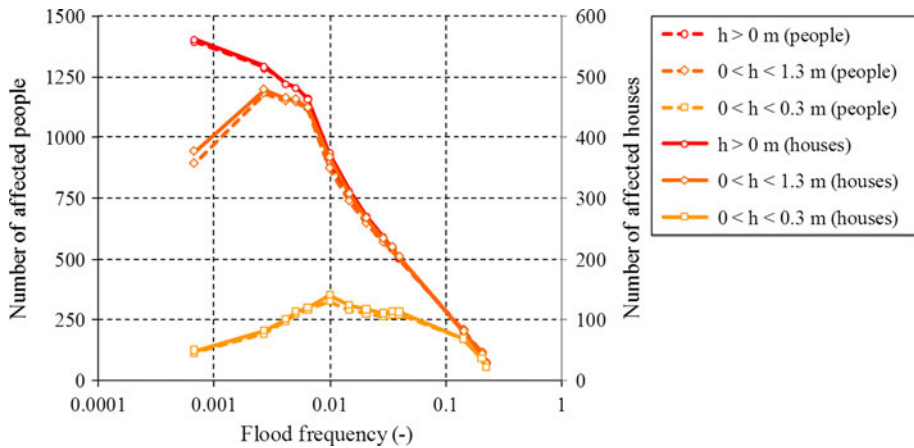
Fig. 7 Exposure expressed by the number of affected people and flooded houses in the downstream reach of the case study, as a function of flood frequency

1.3 m, while a regular increase is found in the number of houses flooded by less than 0.3 m and, even to a greater extent, for those flooded with water depth in-between 0.3 and 1.3 m. In contrast, for discharge values higher than 1000 m³/s, the number of houses flooded by both less than 0.3 m and in between 0.3 and 1.3 m start to decrease, revealing that, for such more extreme events, even buildings located at the edge of the inundation extent undergo flooding with significantly greater water depths.

The procedure also enables to automatically identify and locate all non-residential buildings affected by the floods, as shown in purple in Fig. 6. In this figure, non-residential buildings are numbered, and their exposure is detailed in the list provided in Table 3. Figure 6 reveals notably that affected non-residential buildings include two schools, one home for elderly people, petrol stations as well as sport facilities.

Field surveys along the downstream reach of the case study confirmed that those results of the exposure analysis are indeed almost exhaustive (Boquet 2009). Those buildings are currently considered as hotspots with respect to social impacts, but they are not yet incorporated in the economic damage evaluation. Therefore, they are only analysed in terms of exposure, as shown in Tables 3 and 4, which provide the inundation depth as a function of the flood frequency (or return period) as well as the annual expected value of water depth.

Results discussed in this section tend to demonstrate that the exposure analysis itself provides information of high interest for flood management, with the advantage that these results remain insensitive to additional uncertainties resulting from assumptions underlying the subsequent socio-economic impact analyses.

5.2.3 Social impact

For river Ourthe, the typical floods may be considered as slow and long. Hence, D and WR scores were set, respectively, to 1 and 0 in Eq. 2. Next, applying Eq. 4 for each affected house individually enables to plot social impact maps, as shown in Fig. 8. Such maps may prove helpful to prioritize social vulnerability reduction measures.

Table 3 Inundation depth (m) in non-residential buildings, with the canal rehabilitated (first line) and in the base scenario (second line, *italic*)

Return period	4	5	7	25	29	34	48	68	100	154	196	239	371	1481
Campsite	0.03	0.03	0.13	0.52	0.56	0.62	0.71	0.80	0.90	1.01	1.07	1.12	1.23	1.54
	0.08	*0.10*	*0.20*	*0.62*	*0.66*	*0.71*	*0.80*	*0.88*	*0.98*	*1.09*	*1.14*	*1.20*	*1.30*	*1.60*
Church				0.06	0.08	0.11	0.17	0.26	0.36	0.48	0.55	0.59	0.73	1.09
				0.12	*0.14*	*0.19*	*0.28*	*0.38*	*0.49*	*0.61*	*0.68*	*0.75*	*0.88*	*1.23*
Old people' home	0.01	0.01	0.04	0.25	0.28	0.32	0.38	0.45	0.53	0.64	0.71	0.75	0.87	1.19
	0.01	*0.01*	*0.05*	*0.26*	*0.29*	*0.33*	*0.40*	*0.46*	*0.56*	*0.67*	*0.73*	*0.79*	*0.90*	*1.22*
School 1				0.00	0.00	0.01	0.02	0.03	0.06	0.09	0.10	0.11	0.21	0.43
				0.00	*0.01*	*0.01*	*0.02*	*0.05*	*0.07*	*0.10*	*0.12*	*0.13*	*0.26*	*0.48*
School 2												0.01	0.11	0.43
											0.01	*0.03*	*0.19*	*0.50*
Sport facility 1				0.25	0.84	0.91	1.00	1.15	1.29	1.45	1.62	1.71	1.79	1.96
	0.16	*0.20*	*0.36*	*1.02*	*1.09*	*1.17*	*1.31*	*1.44*	*1.59*	*1.76*	*1.85*	*1.93*	*2.10*	*2.54*
Sport facility 2				0.11	0.70	0.77	0.86	1.00	1.14	1.30	1.47	1.56	1.63	1.80
	0.03	*0.07*	*0.23*	*0.88*	*0.94*	*1.03*	*1.16*	*1.29*	*1.44*	*1.61*	*1.69*	*1.77*	*1.94*	*2.37*
Sport facility 3				0.55	0.61	0.69	0.82	0.96	1.12	1.30	1.39	1.48	1.66	2.16
			0.11	*0.77*	*0.84*	*0.92*	*1.05*	*1.20*	*1.36*	*1.54*	*1.64*	*1.72*	*1.91*	*2.39*
Sport facility 4				0.18	0.91	0.97	1.04	1.16	1.28	1.42	1.56	1.64	1.71	1.88
	0.05	*0.11*	*0.43*	*1.08*	*1.14*	*1.21*	*1.32*	*1.43*	*1.55*	*1.70*	*1.78*	*1.86*	*2.04*	*2.46*
Sport facility 5				0.02	0.30	0.33	0.37	0.43	0.49	0.57	0.66	0.70	0.74	0.83
		0.00	*0.09*	*0.38*	*0.41*	*0.45*	*0.51*	*0.58*	*0.65*	*0.74*	*0.78*	*0.82*	*0.92*	*1.16*
Sport facility 6												0.00	0.02	0.30
										0.00	*0.02*	*0.04*	*0.13*	*0.44*
Sport facility 7				0.07	0.56	0.61	0.68	0.80	0.92	1.06	1.20	1.29	1.35	1.51
	0.03	*0.04*	*0.19*	*0.71*	*0.77*	*0.84*	*0.95*	*1.06*	*1.19*	*1.34*	*1.42*	*1.49*	*1.66*	*2.09*
Petrol station 1											0.00	0.01	0.05	0.38
									0.00	*0.00*	*0.01*	*0.03*	*0.10*	*0.44*
Petrol station 2								0.07	0.17	0.29	0.36	0.41	0.52	0.88
							0.01	*0.11*	*0.22*	*0.35*	*0.41*	*0.47*	*0.59*	*0.95*

Besides the identification of social hotspots, results of the social impact analysis for housing may be plotted in the form of risk curves, as displayed in Fig. 9. Since these results show the relationship between intensity of social impacts and flood frequency, they constitute indeed an expression of the social risk. They indicate, for instance, that a 100-year flood leads to about 300 people weakly socially affected and 580 additional people affected by a medium social impact. They also reveal that none in the floodplains along the considered reaches of river Ourthe encounters a high social impact.

5.2.4 Economic damage

The economic damage analysis is conducted in two steps, focusing here on direct damage to residential buildings. First, combining the results of the exposure analysis with the

Table 4 Annual expected value of inundation depth (m) in non-residential buildings, in the base scenario and with the canal rehabilitated

	Base scenario	Canal rehabilitated	Absolute difference	Relative difference (%)
Campsite	0.102	0.079	0.024	23
Church	0.041	0.039	0.002	5
Old people's home	0.002	0.002	0.000	19
School 1	0.128	0.096	0.032	25
School 2	0.167	0.119	0.048	29
Sport facility 1	0.002	0.001	0.001	40
Sport facility 2	0.002	0.002	0.000	18
Sport facility 3	0.102	0.079	0.024	23
Sport facility 4	0.041	0.039	0.002	5
Sport facility 5	0.002	0.002	0.000	19
Sport facility 6	0.128	0.096	0.032	25
Sport facility 7	0.167	0.119	0.048	29
Petrol station 1	0.002	0.001	0.001	40
Petrol station 2	0.002	0.002	0.000	18
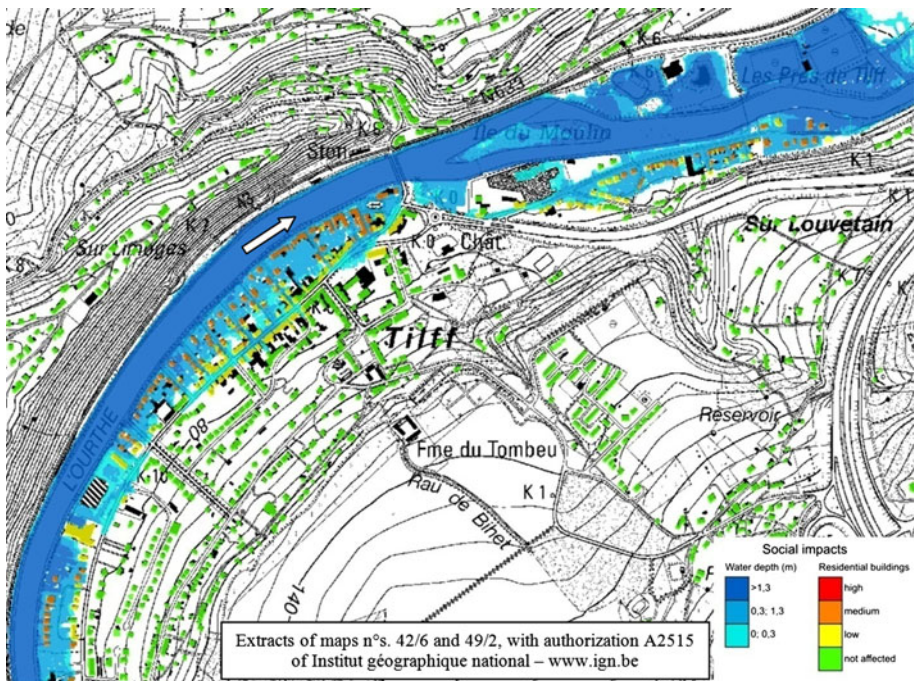
Fig. 8 Spatial distribution of inundation depth (m, *blue colour scale*) and level of social impact (*yellow* to *red colour scale*) for a 154-year flood in the present situation

damage functions (Subsect. 4.3), the relative damage caused by the flood is obtained. Next, based on the estimated house values as a function of their cadastral income, relative damages have been directly converted into absolute ones.
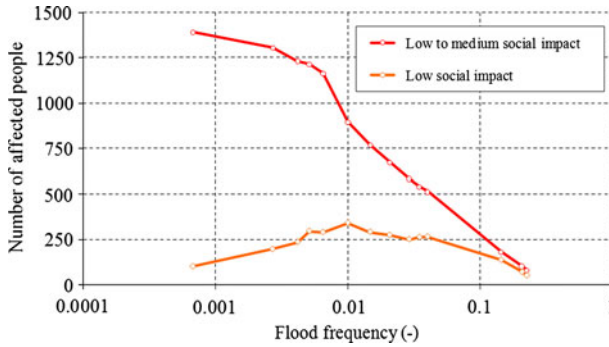
Fig. 9 Social risk, expressed as the number of affected people in each category of social impact as a function of flood frequency (reach no 2 of the case study)

An estimated value of the houses was obtained in the form of a quadratic polynomial function of the cadastral income (Subsect. 4.1). The coefficients were fitted using a sample of property prices obtained from estate agents for houses located in Tilff and Esneux: $P = 160,000 + 50\ CI + 0.125\ CI^2$, where $P(\text{€})$ designates the estimated property price and $CI(\text{€})$ represents the cadastral income. In contrast with meso- and macro-scale analyses, the property price is estimated here for individual buildings and not through a specific price per unit of residential surface (e.g. ICPR 2001).

Figure 10 represents the damage compared to the damage induced by the 100-year flood. More in-depth discussions of socio-economic impacts are presented separately (Coninx and Bachus 2007; Dewals et al. 2008b; Ernst et al. 2008a, b, 2009b), whereas the scope of the present paper concentrates on the integrated methodology and the overall flow of data within the exposure and risk analyses.

5.3 Risk reduction as a result of flood protection measures

The whole risk analysis procedure has been applied to appreciate the efficiency of two flood reduction measures, namely the rehabilitation of an ancient canal and the increase in
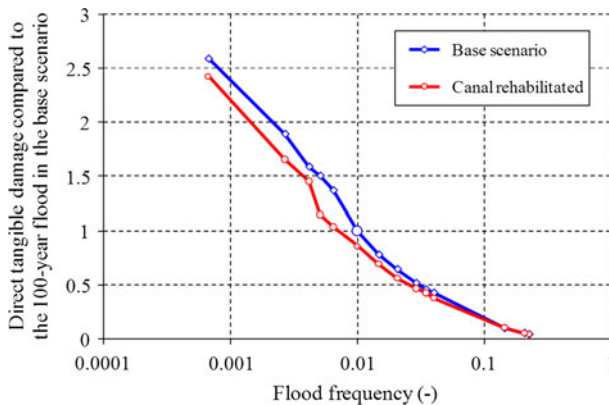
Fig. 10 Economic risk curve for residential buildings, expressed by the direct economic damage compared to the direct economic damage for the 100-year flood (reach no 2 of the case study)

discharge capacity of a floodplain. Such kind of measures was selected mainly due to the relatively limited storage capacity of the floodplains, making them unable to act effectively as temporary retention areas.
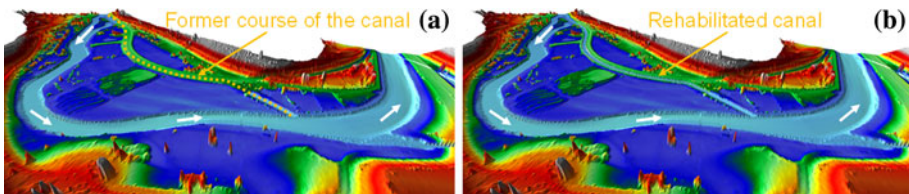
5.3.1 Rehabilitation of an ancient canal

With the support of King William I of the Netherlands, a huge engineering project was initiated at the beginning of the nineteenth century to construct a navigable waterway linking river Ourthe in the Meuse basin to river Moselle in the Rhine basin and crossing the Ardennes massif. For this purpose, a canal was built along several reaches of river Ourthe, including the case study area considered here. The project was never completed but some parts of the canal were used for inland navigation until early in the twentieth century. Although the canal has been partly filled in over the years, many remains are still visible today, such as for instance a lock illustrated in Fig. 11. Based on historical maps and field surveys, the course of the ancient canal has been identified accurately and its section (width and depth) has been estimated. Next, considering the rehabilitation of the canal as a flood protection measure increasing the effective cross-section of the river, the digital surface model used for hydraulic modelling has been updated to introduce the former course of the canal in the topography data used for hydraulic modelling (Fig. 12).
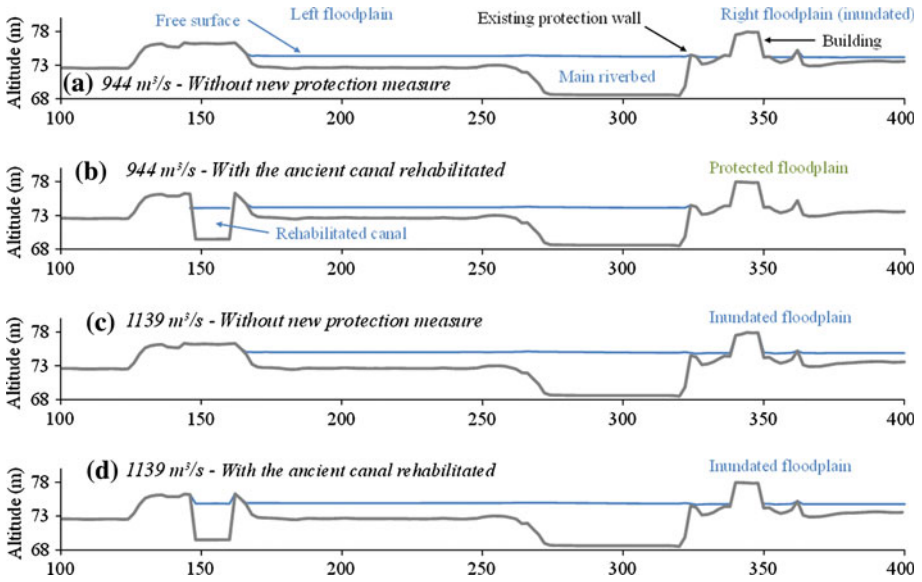
Figure 13 represents a typical cross-section of river Ourthe downstream from Tilff, along with the free surface elevation computed for two different discharges (944 and 1139 m^3/s), both without and with the rehabilitated ancient canal. In the former case, the right floodplain is inundated for both discharges in spite of an existing wall designed to protect a residential district up to the 100-year flood (876 m^3/s). In contrast, as a result of

Fig. 11 Example of a lock along the ancient canal of river Ourthe: (**a**) past and (**b**) present situations. The same building can be identified on the right of both pictures


Fig. 12 3D view of the topography used for hydraulic modelling: (**a**) prior and (**b**) after rehabilitation of the ancient canal

Fig. 13 Typical cross-section (——) of river Ourthe in the case study area as well as corresponding free surface (——) for two different discharges (**a, b**: 944 m³/s; **c, d**: 1139 m³/s) in the present situation (**a, c**) and considering the ancient canal rehabilitated (**b, d**)

the increase by 18% in the available cross-section of the river when the canal is rehabilitated, the protection wall is not overtopped anymore and the right floodplain is protected from flooding. Nevertheless, for the higher discharge value overtopping of the protection wall is not prevented by the rehabilitated canal and this protection measure is thus found to remain effective only for a limited range of discharge values, as detailed later.

To provide more insight into the hydraulic effect of the measure, the spatial distribution of the difference in water elevation between the base scenario and the scenario with the canal rehabilitated is shown in Fig. 14 for four return periods. In all four cases, the
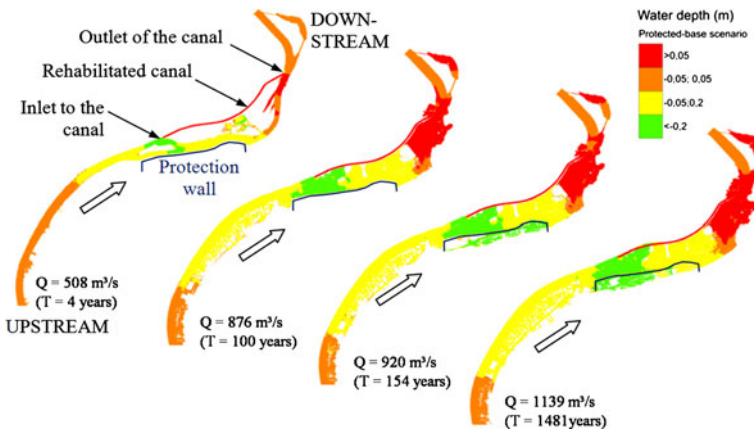
Fig. 14 Difference in water depth (m) between the scenario with the ancient canal rehabilitated and the base scenario

maximum reduction in water depth occurs in the vicinity of the inlet to the canal, whereas an increase in water depth is observed at the outlet of the canal. This increase results from a local decrease in flow velocity, while the head remains constant.

It may be concluded that for all return periods, there is a spatial shift in flood hazard, which decreases near the canal inlet and increases near the canal outlet. In addition, for return periods in the range 100 to about 200 years, inundation is found to be considerably reduced in the area surrounded by the protection wall.

For a 154-year flood, Figs. 6 and 15 compare the inundation depth (blue scale) and the exposure of individual buildings (colour scale yellow to red), expressed by the water depth assigned to each building. The detailed spatial distribution of the change in inundation depth and exposure reveals that (1) in the upstream part, a moderate number of buildings are affected by a reduced water depth; (2) overtopping of the protection wall is prevented, leading to a decrease by about one hundred units in the number of affected buildings and (3) the slight increase in inundation extent further downstream does not increase flood exposure since no additional buildings are affected in this area.

Results in terms of number of affected people (Fig. 16) show mainly a shift in the sharp rise in the exposure corresponding to the overtopping of the protection wall. Indeed, while the wall was originally overtopped for discharges higher than the 100-year flood (876 m^3/s), the rehabilitated canal enables to prevent this overtopping for discharges slightly above a 200-year flood. Apart from this shift in the threshold discharge for overtopping of the wall, rehabilitating the canal leads to a decrease in the total number of affected houses by no more
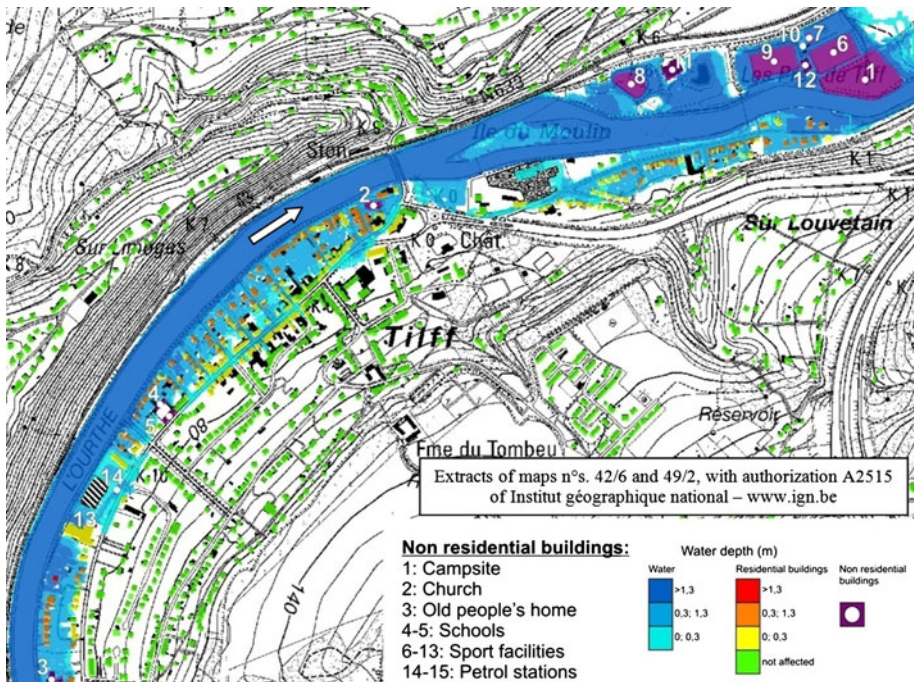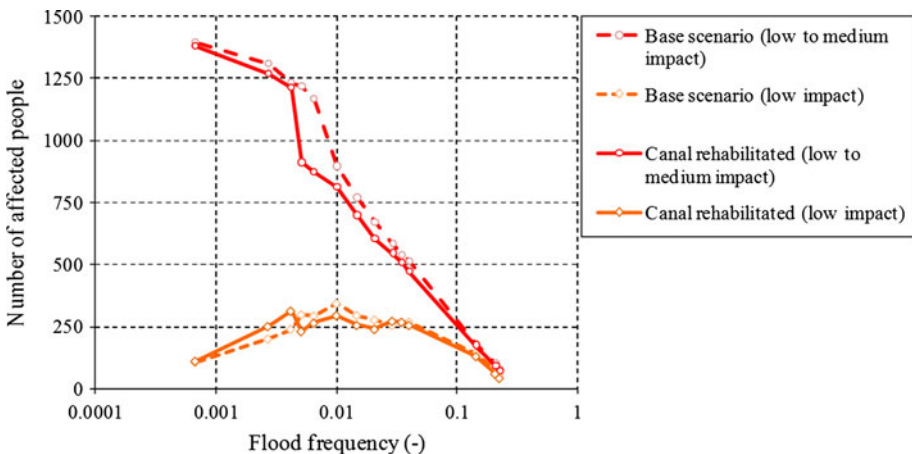

Fig. 15 Spatial distribution of inundation depth (m, *blue colour scale*) and exposure of residential and non-residential buildings (*yellow* to *red colour scale*), for a 154-year flood and considering the rehabilitation of the ancient canal
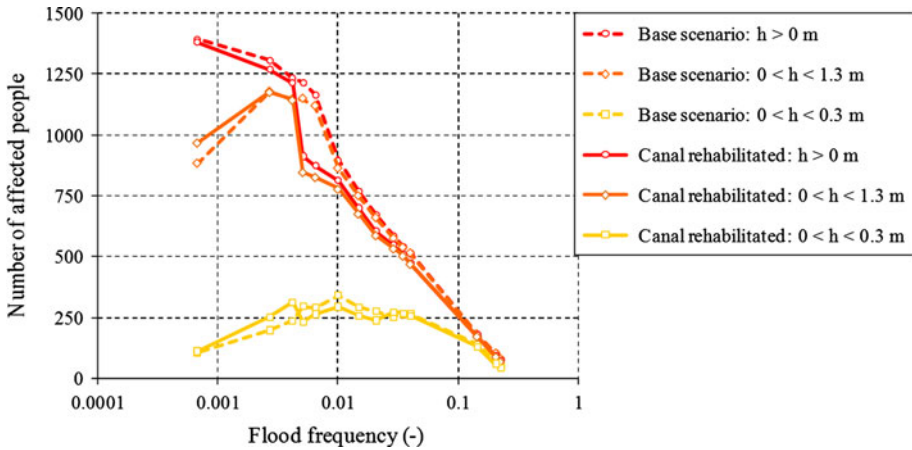
Fig. 16 Influence of the rehabilitated ancient canal on the exposure, expressed as the number of affected people

than 10–20 units. Since the number of inhabitants per house hardly changes in this part of the case study, the corresponding conclusion applies for the number of affected people (Fig. 16), as well as for social impact (Figs. 17, 18).

The decrease in direct economic damage to housing is found to reach 10–15% of initial damage for the whole range of discharges, except for return periods in-between 100 and approximately 200, for which the relative reduction in damage becomes as high as 25%. Integrating the economic risk curve, using Eq. 1, leads to an annual avoided risk of about 40 k€. The investment, maintenance and operation costs of the measure should be balanced with this figure, as well as with the avoided social risk. Thereby, tangible decision-support information may be provided to policy makers regarding the efficiency of the measure, which effectively reduces flood impacts only in a restricted range of discharge.

Fig. 17 Influence of the rehabilitated ancient canal on the social risk curves
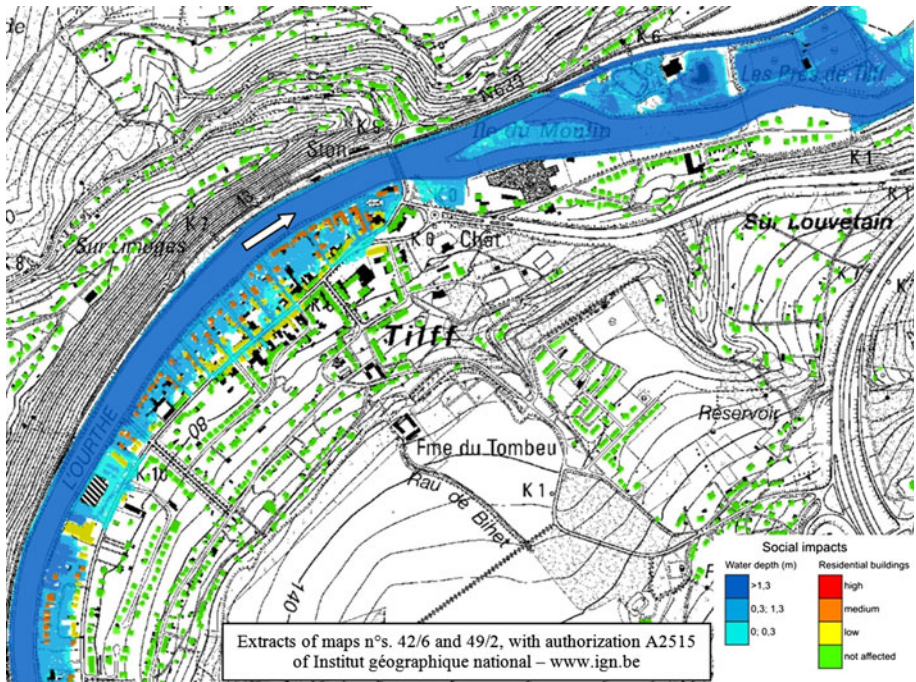
Fig. 18 Spatial distribution of inundation depth (m, *blue colour scale*) and level of social impact (*yellow to red colour scale*), for a 154-year flood and considering the rehabilitation of the ancient canal
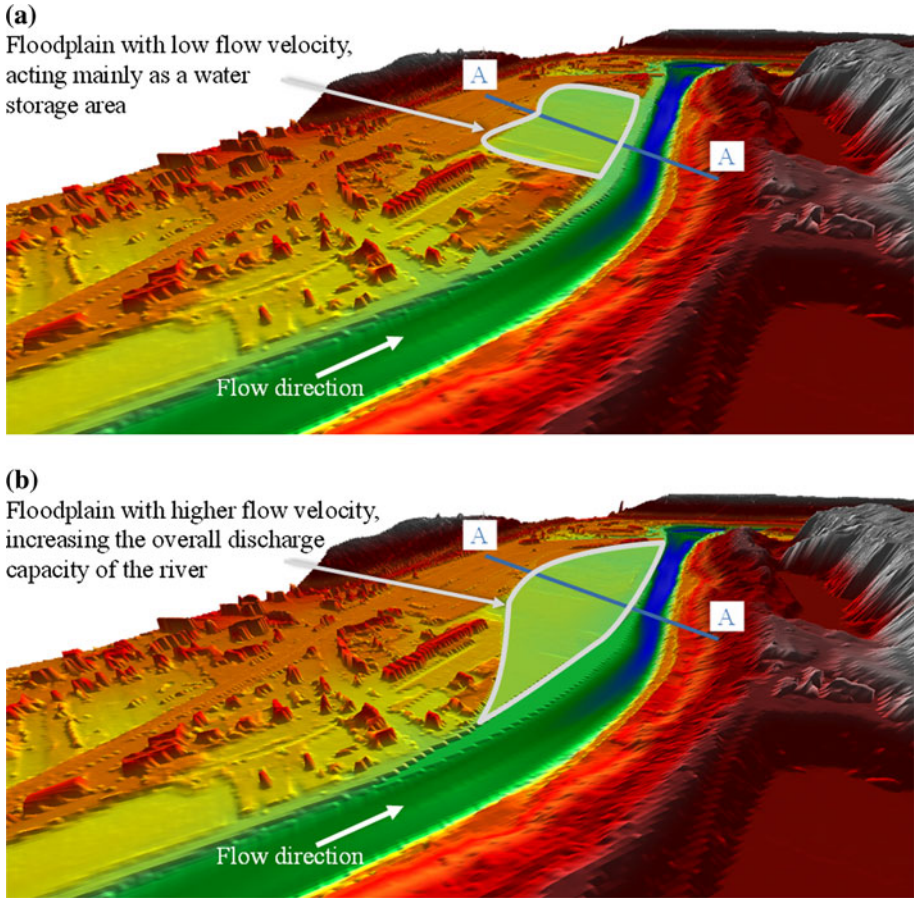
5.3.2 Increase in the discharge capacity of floodplains

The second adaptation measure considered here consists in recalibrating the topography of a non-urbanized floodplain in reach no 1 of the case study (Fig. 3), in such a way that the overall local discharge capacity increases, resulting in a decrease in water depth in an urbanized floodplain located upstream.

As shown in Fig. 19, the changes in the topography of the floodplain, originally characterized by low flow velocity (Fig. 20), enable eventually the development of higher flow velocities beyond the main riverbed (Figs. 21, 22). As a result, the effective width of the river is increased and, consequently, the water level in the floodplain upstream is found to be reduced by 40 cm in the case of a 100-year flood. The detailed 2D hydraulic modelling approach is particularly suitable for predicting the effect of such a measure, since it enables to properly reproduce the cross-distribution of velocity in the dynamically interacting main riverbed and floodplains.

For steady flow conditions, the hydraulic model reveals no changes in the water depths computed downstream of the modified topography. Therefore, the results of the exposure analysis are presented only for the urbanized floodplain immediately upstream of the recalibrated one (Figs. 23, 24). In addition, since the area of interest is entirely included within a single statistical sector, the number of inhabitants per house is assumed to be uniform in the whole area. Hence, only the number of affected buildings is detailed in Fig. 23, while the number of affected people is simply 2.7 times higher. In contrast with rehabilitating the ancient canal, modifying the floodplain topography is shown to lead to a

Fig. 19 3D view of topography in the upstream considered reach of river Ourthe, (**a**) in the base scenario and (**b**) after topography changes to increase discharge capacity in the left floodplain. The extent of the floodplain is highlighted in each figure, as well as cross-section AA for which velocity distribution is shown in Fig. 21
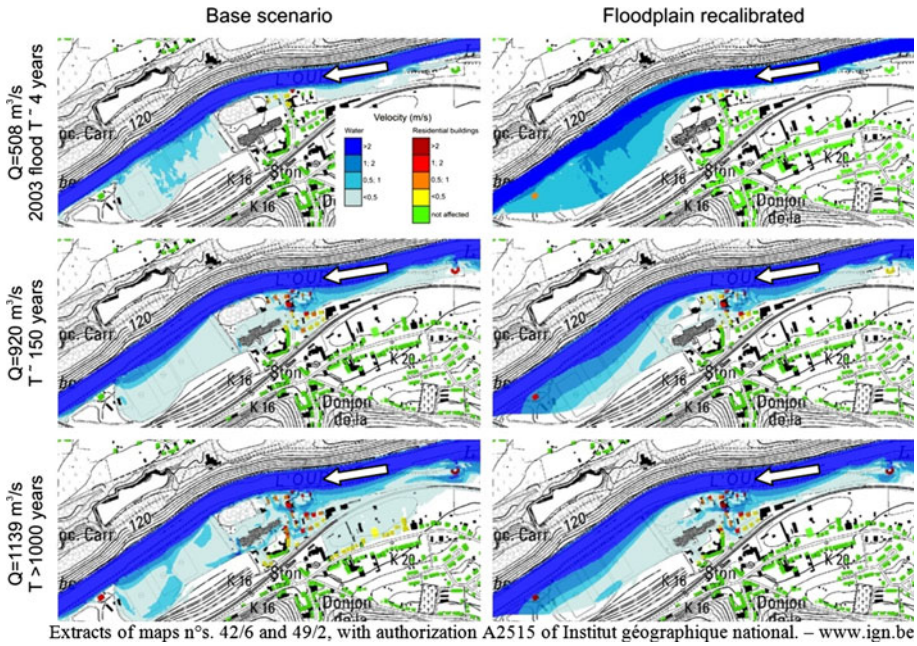
Fig. 20 Aerial photography of the considered passive floodplain along river Ourthe during a flood in February 2002 (570 m³/s)
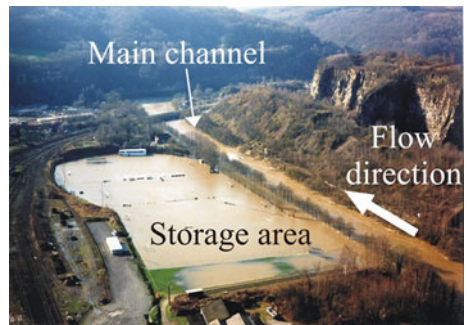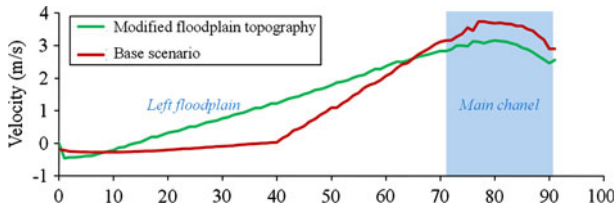
Fig. 21 Cross-sectional distribution of flow velocity in the base scenario and considering a change in the topography of a floodplain in the upstream reach of the case study


Fig. 22 Spatial distribution of flow velocity (m/s) in the river and the floodplains (*blue colour scale*), as well as velocity values assigned the each residential building (*yellow* to *red colour scale*)

significant decrease in the exposure for the whole range of discharges. Moreover, the higher the discharge, the more effective is the protection measure, especially in areas characterized by high water depth, both in terms of exposure and social impact (Fig. 24).

The spatial distribution of water depth and social impact is detailed in Fig. 25 for three representative different return periods. Comparison of the subfigures in the left and right columns enables to precisely locate the buildings which get unaffected as a result of the floodplain recalibration, as well as those which undergo a lower social impact. The difference is particularly obvious for the highest considered flow rate.

6 Conclusion

The present paper describes the combination of a detailed two-dimensional hydraulic model with a procedure for the analysis of flood exposure and the appreciation of flood risk
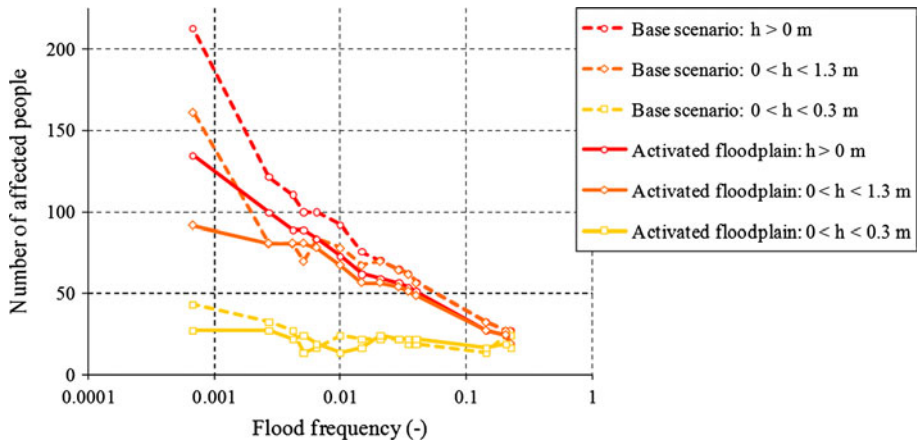
Fig. 23 Influence on the exposure of changes in topography of a floodplain in the upstream reach of the case study, expressed as the number of affected people as a function of the discharge
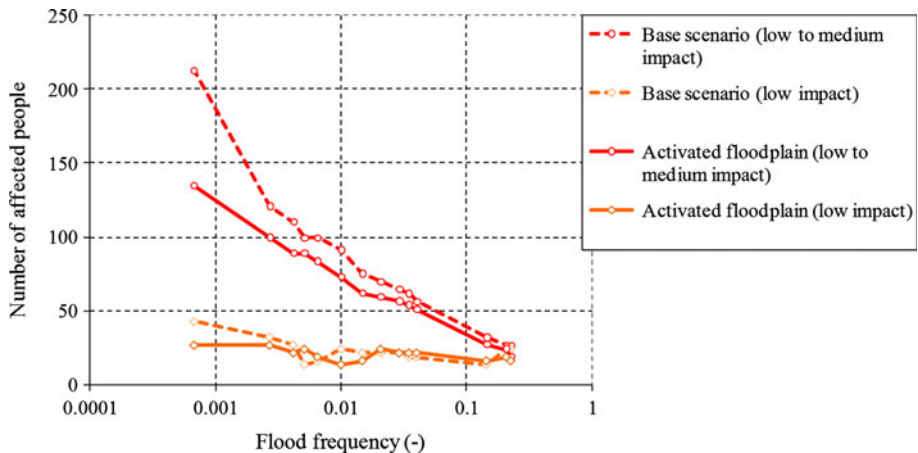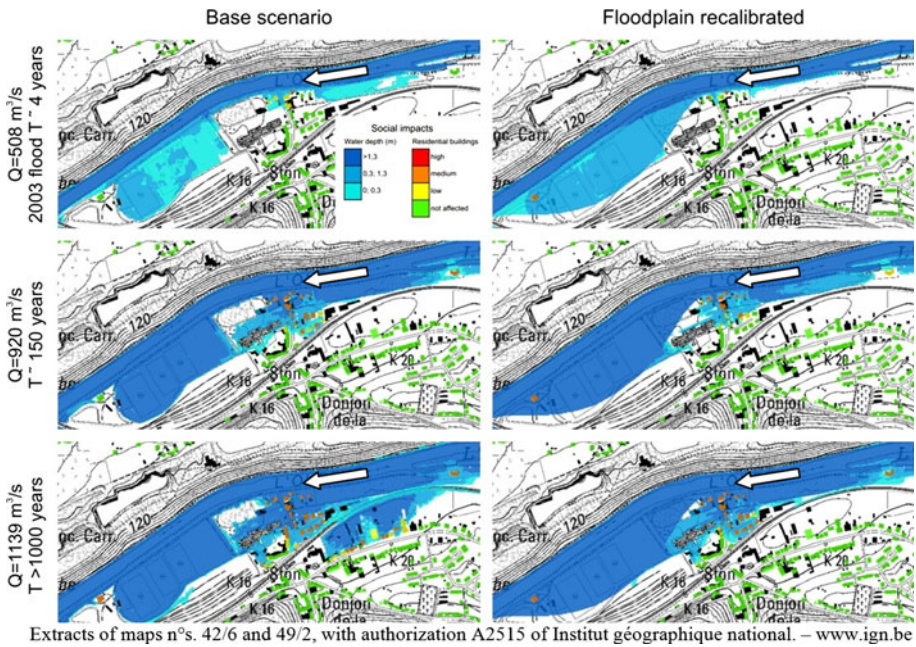

Fig. 24 Influence of the activated passive floodplain on the social risk curve

at a micro-scale. The hydraulic model succeeds in predicting accurately the pattern of water depth in urbanized floodplains for a wide range of flood discharges without the need for recalibration of the roughness coefficient.

The methodology relies on a consistent approach in terms of accuracy of input data, hydraulic modelling and expected results. Indeed, besides detailed hydraulic modelling conducted on computational grids as fine as 2 m by 2 m, exploited data include laser altimetry (LIDAR), high resolution and high quality land use maps as well as other complementary vector geographic datasets providing socio-economic information at a micro-scale. Results are provided notably in the form of detailed maps showing the spatial distribution of flood hazard and exposure for individual building.

Next to flow modelling and exposure analysis conducted for each building or facility individually, the procedure involves social impact analysis and the evaluation of direct economic damage based on a standard relative damage function. Thanks to the micro-scale

Extracts of maps n°s. 42/6 and 49/2, with authorization A2515 of Institut géographique national. – www.ign.be

Fig. 25 Spatial distribution of inundation depth (m) in the river and the floodplains (*blue colour scale*), as well as level of social impact (*yellow* to *red colour scale*)

approach, the social impact analysis includes the identification of the exposure of each individual public facility such as schools and hospitals, which constitute social hotspots. The outcomes of the overall analysis were exploited to evaluate the effectiveness of individual flood protection measures.

The applicability of the overall automatic procedure has been demonstrated by the evaluation of inundation hazard, exposure and flood risk for a case study along river Ourthe in the Meuse Basin (Belgium). For validation purpose, recent flood events were first simulated, and a base scenario has been considered. Next, analysis of two flood protection measures has shown a significant difference in the range of discharges for which the measures lead to significant reductions in the inundation impacts.

Application of the methodology to other Belgian rivers is straightforward since necessary data are widely accessible throughout the country. The methodology also applies to other urbanized and semi-urbanized floodplains, provided data on hand are suitable for micro-scale analysis.

References

Apel H, Aronica G, Kreibich H, Thieken A (2007) Flood risk assessment strategies—a comparative study. Geophys Res Abstr 9:02916

Apel H, Aronica G, Kreibich H, Thieken A (2009) Flood risk analyses—how detailed do we need to be? Nat Hazards 49(1):79–98

Bates PD, de Roo APJ (2000) A simple raster-based model for flood inundation simulation. J Hydrol 236:54–77

Begnudelli L, Sanders BF, Bradford SF (2008) Adaptive Godunov-Based model for flood simulation. J Hydraul Eng 134(6):714–725

Boquet A (2009) Contributions à l'analyse du risque d'inondation : probabilité de rupture de barrage et enquête de validation de dommages, University of Liège, 74

Bradbrook K, Waller S, Morris D (2005) National floodplain mapping: datasets and methods—160,000 km in 12 months. Nat Hazards 36(1):103–123

Brouwer R, Akter S, Brander L, Haque E (2007) Socioeconomic vulnerability and adaptation to environmental risk: a case study of climate change and flooding in Bangladesh. Risk Anal 27(2):313–326

Caleffi V, Valiani A, Zanni A (2003) Finite volume method for simulating extreme flood events in natural channels. J Hydraul Eng-ASCE 41(2):167–177

Chaudhry MH (1993) Open-channel flow. Englewood Cliffs, Prentice Hall

Coninx I (2008) Social flood risk assessment—methodological paper for the ADAPT project. Leuven, KUL, 25

Coninx I, Bachus K (2007) Integrating social vulnerability to floods in a climate change context. In: Proc. int. conf. on adaptive and integrated water management, coping with complexity and uncertainty, Basel, Switzerland

de Wit MJM, Peeters HA, Gastaud PH, Dewil P, Maeghe K, Baumgart J (2007) Floods in the Meuse basin: event descriptions and an international view on ongoing measures. Int J River Basin Manage 5(4):279–292

Dewals BJ, Erpicum S, Archambeau P, Detrembleur S, Pirotton M (2006a) Depth-integrated flow modelling taking into account bottom curvature. J Hydraul Res 44(6):787–795

Dewals BJ, Erpicum S, Archambeau P, Detrembleur S, Pirotton M (2006b) Numerical tools for dam break risk assessment: validation and application to a large complex of dams. In: Hewlett H (ed) Improvements in reservoir construction, operation and maintenance. Thomas Telford, London, pp 272–282

Dewals BJ, Detrembleur S, Archambeau P, Erpicum S, Pirotton M (2008a) Detailed 2D hydrodynamic simulations as an onset for evaluating socio-economic impacts of floods considering climate change. In: Samuels P, Huntington S, Allsop W, Harrop J (eds) Flood risk management: research and practice. Taylor & Francis, London, pp 125–135

Dewals BJ, Giron E, Ernst J, Hecq W, Pirotton M (2008b) Integrated assessment of flood protection measures in the context of climate change: hydraulic modelling and economic approach. In: K Aravossis, CA Brebbia, N Gomez (eds) Environmental economics. WIT press, Southampton, UK, p 10

Dewals BJ, Kantoush SA, Erpicum S, Pirotton M, Schleiss AJ (2008c) Experimental and numerical analysis of flow instabilities in rectangular shallow basins. Environ Fluid Mech 8:31–54

Dushmanta D, Srikantha H, Katumi M (2003) A mathematical model for flood loss estimation. J Hydrol 277:24–49

Ernst J, Dewals BJ, Detrembleur S, Archambeau P, Erpicum S, Pirotton M (2008a) Integration of accurate 2D inundation modelling, vector land use database and economic damage evaluation. In: Samuels P, Huntington S, Allsop W, Harrop J (eds) Flood risk management: research and practice. Taylor & Francis, London, pp 1643–1653

Ernst J, Dewals BJ, Giron E, Hecq W, Pirotton M (2008b) Integrating hydraulic and economic analysis for selecting flood protection measures in the context of climate change. In: Proc. 4th int. symp. on flood defence, Toronto, Canada, Institute for Catastrophic Loss Reduction

Ernst J, Coninx I, Dewals BJ, Detrembleur S, Erpicum S, Bachus K, Pirotton M (2009a) Social flood impacts in urban areas: integration of detailed flow modelling and social analysis. In: Proc. 33rd IAHR congress—water engineering for a sustainable environment. Vancouver, British Columbia, IAHR

Ernst J, Coninx I, Dewals BJ, Detrembleur S, Erpicum S, Pirotton M, Bachus K (2009b) Planning flood risk reducing measures based on combined hydraulic simulations and socio-economic modelling at a micro-scale. In: Proc. European water resources association 7th int. conf.—water resources conservation and risk reduction under climatic instability, Limassol, Cyprus

Erpicum S, Archambeau P, Detrembleur S, Dewals B, Pirotton M (2007) A 2D finite volume multiblock flow solver applied to flood extension forecasting. In: García-Navarro P, Playán E (eds) Numerical modelling of hydrodynamics for water ressources. Taylor & Francis, Londres, pp 321–325

Erpicum S, Dewals BJ, Archambeau P, Pirotton M (2009a) Dam-break flow computation based on an efficient flux-vector splitting. J. Comput Appl Math (in press). doi:10.1016/j.cam.2009.08.110

Erpicum S, Meile T, Dewals BJ, Pirotton M, Schleiss AJ (2009b) 2D numerical flow modeling in a macro-rough channel. Int J Numer Methods Fluids 61(11):1227–1246

Erpicum S, Dewals BJ, Archambeau P, Detrembleur S, Pirotton M (2010) Detailed inundation modeling using high resolution DEMs. Eng Appl Comput Fluid Mech 4(2):196–208

FloodSite (2005) Language of risk 56

Giron E, Coninx I, Dewals BJ, El Kahloun M, De Smet L, Sacré D, Detrembleur S, Bachus K, Pirotton M, Meire P, De Sutter R, Hecq W (2009). Towards an integrated decision tool for adaptation measures—case study: floods. « ADAPT » Final Report Phase 1. Brussels, Belgian Science Policy, 122

Hervouet J-M (2003) Hydrodynamique des écoulements à surface libre—Modélisation numérique avec la méthode des éléments finis. Paris, Presses de l'école nationale des Ponts et Chaussées

ICPR (2001) Rhine atlas International Commission for the Protection of the Rhine

IPCC (2007) Climate change 2007: Synthesis Report—Summary for policymakers. Intergovernmental Panel on Climate Change

Kaplan S, Garrick BJ (1981) On the quantitative definition of risk. Risk Anal 1(1):11–27

Kreibich H, Müller M, Thieken AH, Merz B (2007) Flood precaution of companies and their ability to cope with the flood in August 2002 in Saxony, Germany. Water Resour Res 43(W03408). doi:10.1029/2005WR004691

McMillan HK, Brasington J (2007) Reduced complexity strategies for modelling urban floodplain inundation. Geomorphology 90(3–4):226–243

McMillan HK, Brasington J (2008) End-to-end risk assessment: a coupled model cascade with uncertainty estimation. Water Resour Res 44(W03419):14

Merz B, Kreibich H, Thieken A, Schmidtke R (2004) Estimation uncertainty of direct monetary flood damage to buildings. Nat Hazards Earth Syst Sci 4(1):153–163

Mignot E, Paquier A, Haider S (2006) Modeling floods in a dense urban area using 2D shallow water equations. J Hydrol 327(1–2):186–199

Penning-Rowsell EC, Johnson C, Tunstall SM, Tapsell SM, Morris J, Chatterton JB, Coker A, Green C (2003) The benefits of flood and coastal defence: techniques and data for 2003. Flood Hazard Research Centre, Middlesex University

Roger S, Dewals BJ, Erpicum S, Pirotton M, Schwanenberg D, Schüttrumpf H, Köngeter J (2009) Experimental und numerical investigations of dike-break induced flows. J Hydraul Res 47(3):349–359

Smith DI (1994) Flood damage estimation—a review of urban stage damage curves and loss function. Water SA 20(3):231–238

Thieken AH, Müller M, Kreibich H, Merz B (2005) Flood damage and influencing factors: new insights from the August 2002 flood in Germany. Water Resour Res 41(W12430). doi:10.1029/2005WR004177

Thieken AH, Ackermann V, Elmer F, Kreibich H, Kuhlmann B, Kunert U, Maiwald H, Merz B, Müller M, Piroth K, Schwarz J, Schwarze R, Seifert I, Seifert J (2008) Methods for the evaluation of direct and indirect flood losses. In: Proc. 4th int. symp. on flood defence, Toronto, Canada, Institue for Catastrophic Loss Reduction

Van der Sande CJ, de Jong SM, de Roo APJ (2003) A segmentation and classification approach of IKONOS-2 imagery for land cover mapping to assist flood risk and flood damage assessment. Int J Appl Earth Observ Geoinf 4:217–229

Wu W (2008) Computational river dynamics. Taylor & Francis, London